International Forum on Aeroelasticity and Structural Dynamics
IFASD 2022
13-17 June 2022, Madrid, Spain

ACTIVE FLUTTER SUPPRESSION OF A HIGHLY FLEXIBLE SWEPT WING THROUGH MULTIPLE FLAP CONTROL

Stefan Waitz[1]

[1] German Aerospace Center (DLR), Institute of Aeroelasticity
Bunsenstr. 10, 37073 Goettingen, Germany
stefan.waitz@dlr.de

Keywords: Aeroelastic stability, active flutter suppression (AFS), aero-servoelasticity (ASE), flap control, slender wings, structural dynamics.

Abstract: Future commercial aircraft designs tend to light-weight wing structures for energy and cost saving reasons. The slenderness and flexibility of these higher aspect-ratio wings might show susceptibility not only to lower flutter flight speeds. Also, the danger of a larger number and variety (e.g. through sweep induced coupling) of potentially wing-dominated flutter modes is impending. The main objective of the submitted work is to depict a suitable control methodology, and show how dynamic stability of highly flexible wings can be achieved by actively influencing the aeroelastic behaviour of the overall deformed structure. On the prediction side, the design, build-up and analysis of aero-servoelastic simulation models become necessary. The incorporation of active control elements like sensors, actuators and controllers leads to closed-loop models. On simulation side, the strategic goal of this investigation is to reach the capability of completely erasing any kind of flutter occurrence, with no restrictions, neither in composition (e.g. heave, torsion, in-plane sway or flap dominated) nor in number (e.g. up to 4) of eigenmodes. The design of the controller transfer functions turned out to be crucial. In order to have the desired variety of eigenmodes at disposal, here a number of three configurations of the nominal generic wing design (baseline with five deflection-controlled flaps plus two modifications) underwent the analyses. By means of active flutter suppression (AFS), formerly unstable wing configurations could be transferred into aeroelastic stable flight conditions at any point of a potential flight envelope.

1 INTRODUCTION

The occurrence of flutter as a hazardous event of elastic structures in flow environment mostly leads to failure and demolition of the aircraft. The loss of flutter stability within a flight envelope of an aircraft can be avoided by shifting these flutter points to higher flight velocities, or by erasing them at all. Beside constructional passive means of flutter mitigation – artificial increase in natural damping or modification in the mass and stiffness distribution – actively flutter affecting sub-systems can be integrated into the design. This could result in the incorporation of active control elements like sensors, actuators and controllers on both sides, the real structure and the simulation model. The instantaneous reactions of the control chain contribute to the self-induced vibrations of the elastic system in flow. Therefore, the aero-servoelastic (ASE) nature of the environment requires closed-loop (CL) simulation models [4-6,12]. In order to beneficially influence the aero-mechanical behaviour of aircraft, active control measures in aeronautics have been applied or are being investigated in different fields. Automatic flight control systems (AFCS) which guarantee stability in maneuver or steady

flight are well established within flight mechanics. Another promising field for the application of control systems are active load alleviation devices, aiming at the reduction of structural loads during gust encounters or flight maneuvers. In this investigation, an approach for the suppression of aeroelastic dynamic instabilities by erasing or, at least, favourably shifting flutter boundaries to higher flight speed regimes is realized, which thus ensures the prevention of eventual loss of aeroelastic stability. The application of discrete actuators, acting on aerodynamic control surfaces, generally allows larger operating displacements in comparison with alternative force introducing approaches, like surface distributed piezo devices.

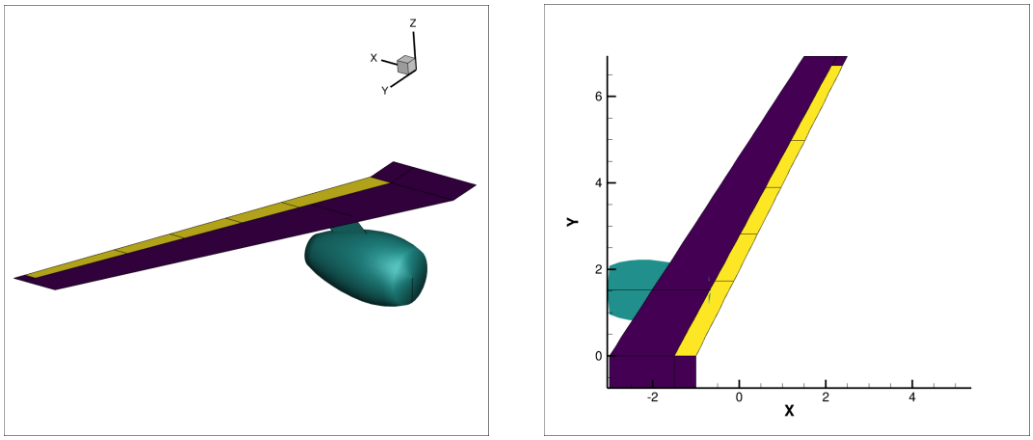

Figure 1: Aerodynamic panel model of control loop equipped ASE-wing, 5 flaps and engine nacelle.

The main objective of the submitted work is to depict a possible control methodology, and show how dynamic stability of highly flexible wings can be achieved by actively influencing the aeroelastic behaviour of the overall deformed structure. On the prediction side, the design, build-up and analysis of aero-servoelastic simulation models becomes necessary. The incorporation of active control elements, like sensors, actuators and controllers leads to closed-loop models. On simulation side, the strategic goal of this investigation is to reach the capability of completely erasing any kind of flutter occurrence, with no restrictions, neither in composition (e.g. heave, torsion, in-plane sway or flap dominated) nor number (e.g. up to 4) of eigenmodes. In order to have the desired variety of eigenmodes at disposal, beside the baseline wing design, two modifications (in total three “configurations”) undergo the analyses in this study, and will be closer described in the following chapters.

2 MODEL BUILD-UP

2.1 Structural Model

In order to determine and counteract eventual flutter cases, a complete aero-servoelastic model of the investigated generic ASE-wing has been built up, developed to systematically undergo the various aeroelastic simulations. Three different wing configurations have been assembled with regard to the structural composition. The investigated wing structure had been built up as a generic wing model, specifically designed for the presented investigation. Nevertheless, single (half) wings like this generalized wind tunnel model, mounted to a wind tunnel side wall and through its structural flexibility suitable, have been and will be used in future aero-servoelastic wind tunnel experiments [7-10]. The distribution of the structural properties of the wing components were determined in a way that enabled the occurrence of various flutter cases. This design approach could be considered as a “reverse” aeroelastic tailoring, with the goal not to prevent, but to enable specific flutter occurrences. The emerging flutter cases were grouped together in clusters in the high subsonic region (< Ma=0.7). The wing sweep (33.0° at the leading edge, 28.4° at the common hinge line of the 5 flaps), an

attached engine nacelle and five controllable flaps along the trailing edge, with a width of 25% of the local chord length, constitute the major design features of the wing model (see Figure 1). The five unbalanced rigid flaps, numbered 1 to 5 from wing root to tip, are attached through pivot points to the elastic wing structure and can either be locked or provided with a finite hinge line stiffness, thus establishing their individual flap eigen frequency. Note, that for reasons of shortness, in this study the term "flap" is used for addressing of all (five) aerodynamic control surfaces (or movable trailing edge devices), all the more that their common purpose here is being applied as aerodynamic surfaces in aero-servoelastic control loops. Nevertheless, the two inner flaps represent (multi-functional or hinged) landing flaps, the two outer ones stand for ailerons, whereas the central one could be considered as being established especially for flutter suppression reasons. The build-up of the unsteady doublet lattice panel grid (DLM), all ASE component modelling and the final solution of the flutter eigenvalue problems were performed with the aeroelastic software package ZAERO [1,2,11,13-14]. Solutions in open and in closed loop (OL, CL) were produced using both, rational function approximations and frequency domain aerodynamics. The reduced structural FE basis of eigenmodes had been imported into the aero-servoelastic solver from NASTRAN.

2.2 Model Configurations

Furthermore, three wing model configurations have been defined to achieve a larger variety in composition of the eigenmodes (i.e. with varying dominant components of the respective mode shape). Starting from the baseline design, the three configurations differed in the global parameters "pitch angle" and "flap hinge stiffness" (see Table 1), while they showed no differences in the respective aerodynamic panel grids. Note that the used term "pitch angle" here refers to the structural incidence setting, i.e. the structural properties had been rotated by the respective angle settings, resulting in a structural coupling between (out-of-plane) heave and (in-plane) sway motion. As usual in linear flutter analyses, no static lift deformation had been taken into account, and the DLM grid panels, describing the aerodynamic disturbance variables, remained unchanged for the three wing model configurations. Summarizing the motivation for introducing the wing model by these three configurations, it can be stated that this approach opened the possibility (1.) to achieve a larger variety of eigenmodes, (2.) to keep the wing structure unchanged (mass and stiffness) and (3.) to roughly preserve an "upward compatibility" of the flutter eigenmodes between the three configurations.

Table 1: Model parameters (structural wing pitch setting and flap hinge stiffness) of three wing model configurations.

Wing model	Structural pitch angle setting	Flap hinge stiffness	No. of emerging flutter modes
Configuration I	0°	fixed	1, 2
Configuration II	+15°	fixed	1, 2, 3
Configuration III	+15°	flexible	1, 2, 3, 4

Representing the main structural dynamic behaviour of the wing model, the eigenfrequencies of wing configuration III are presented in Table 2. Regardless of minor participation of the other components, caused by geometric coupling through the structural pitch and the wing sweep angle, the denoted mode characterizations refer to the dominant mode components. The eigenfrequencies coincide with each other for the lower modes of the three configurations, but differ for modes with significant flap deflection participation (e.g. mode 7 and 8), being enabled by the finite stiffness (flexibility) of the flap hinges. In the flutter calculations of both, the open- and the closed-loop analyses a modal basis of 30 eigenmodes

had been used, covering a frequency range of up to 500 Hz in the case of the fixed hinges (configuration I and II), and up to 400 Hz in the flexible flap hinge case (configuration III).

Table 2: The lower structural modes and wing eigenfrequencies of configuration III.

Number	Frequency [Hz]	Mode		Number	Frequency [Hz]	Mode
1.)	1.29	1. Heave		5.)	25.5	3. Heave
2.)	4.64	1. Sway		6.)	30.3	2. Sway
3.)	8.41	2. Heave		7.)	32.2	1. Flaps
4.)	22.5	1. Torsion		8.)	37.6	2. Flaps

3 OPEN-LOOP FLUTTER BEHAVIOUR

3.1 Flutter Modes

Prior to the closed-loop ASE calculations, the wing model underwent conventional flutter analyses. By comparing the flutter results of the open-loop simulations (for the flutter diagrams of configuration I and III, see Figure 6 and 10, respectively), the number and character of the emerging flutter cases could be confirmed. The quantity of flutter modes which appeared for the three wing configurations, and which have been dealt with in this flutter suppression study, are depicted in Figure 2. They are numbered from 1 to 4 and characterized by their dominant deformation components: Heave, torsion, sway and flaps. Nevertheless, in each flutter mode all other components are contained, though to a minor degree of participation (for instance small, but considerable torsional components in the in-plane swaying mode).

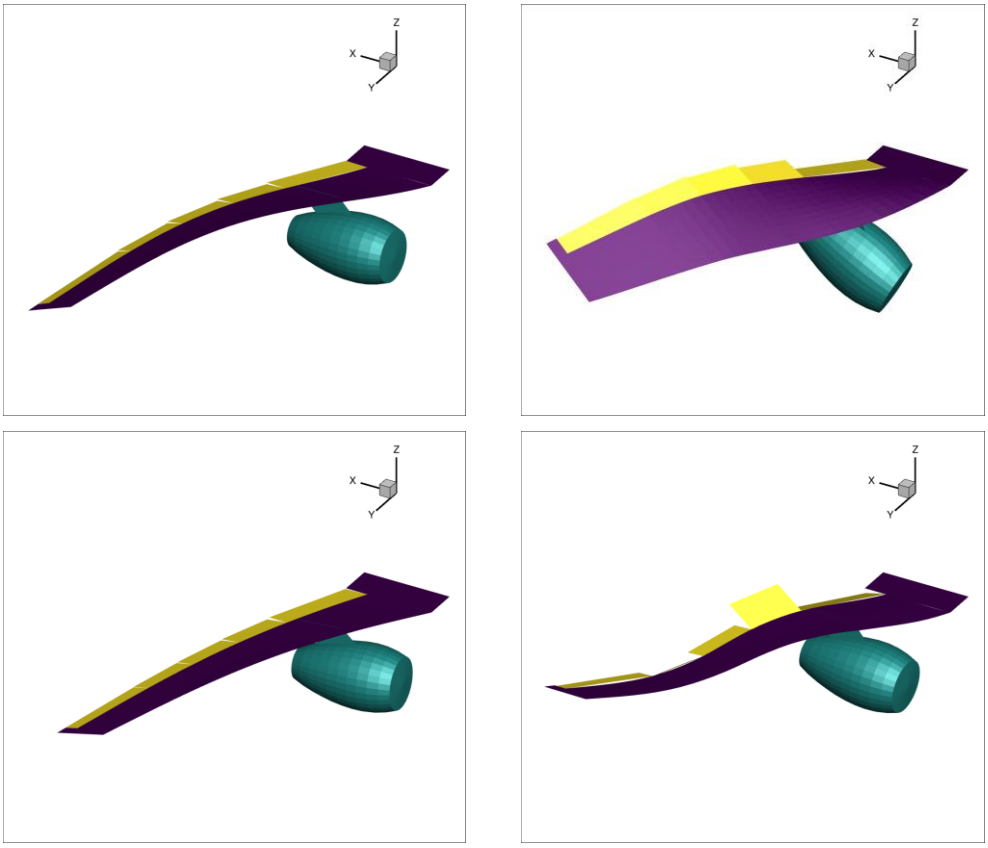

Figure 2: Flutter mode 1 (HEAVE, upper left), flutter mode 2 (TORSION, upper right), flutter mode 3 (SWAY, lower left) and flutter mode 4 (FLAPS, lower right) of configuration III.

3.2 Flutter Cases

Looking at the numerical values of flutter frequency and flutter speed for each of the three wing configurations (see Table 3 and 4), the criteria of model "up-ward" compatibility for the flutter modes (configuration II as subset of III, and configuration I as subset of II or III) could be confirmed. Beside the advantage of an evident classification and grouping, the close affinity of the modes within the three wing configurations also allowed a common treatment w.r.t the control parameters (for instance same gain values in the control loops).

Table 3: Flutter frequencies of all 3 wing model configurations.

Flutter frequency [Hz]	Flutter mode 1 HEAVE	Flutter mode 2 TORSION	Flutter mode 3 SWAY	Flutter mode 4 FLAPS
Configuration I	6.786	14.15	/	/
Configuration II	6.827	13.57	4.440	/
Configuration III	6.945	13.34	4.439	33.03

Table 4: Flutter speeds of all 3 wing model configurations.

Flutter speed [m/sec]	Flutter mode 1 HEAVE	Flutter mode 2 TORSION	Flutter mode 3 SWAY	Flutter mode 4 FLAPS
Configuration I	163.1	151.6	/	/
Configuration II	167.8	156.3	146.7	/
Configuration III	167.9	152.0	145.4	238.0

4 CONTROL ARCHITECTURE

4.1 Control Loop Structure

A complete control environment had been added to the structural and aerodynamic wing parts, to result in the final aero-servoelastic simulation model. These ASE elements comprise sensors, actuators, controllers and gain components for each of the five aerodynamic control surfaces (see Figure 3). With their help, all of the control surfaces (or a sub-set out of the 5 wing flaps) can be addressed individually by structural sensor data (e.g. wing deformations or accelerations), to be well chosen to counteract the flutter modes and thus, prevent instable flight conditions. In the final closed-loop flutter calculations (with controller type 2, see Chapter 5.3 and 5.4), the rotational acceleration of the airfoil around the global y-axis, β'', measured on each control surface, constitute the individual sensor signal for each flap (collocated feedback). Consequently, the acceleration sensor signals comprise both, the elastic airfoil pitch deformation plus the flap deflection (elastic and control share) at the respective spanwise sensor position. In contrast to these, the flap deflection angles δ_i, measured around the hinge axis and relative to the elastic flap deformation, serve as control variables. The controller design primarily consists of defining the shape of the flap controllers by finding suitable rational function expressions for the controller transfer functions (TF). Secondly, the corresponding parameters have to be determined to fulfill the aimed target of abolishing the flutter instabilities, e.g. in a semi-automatized search. Basic to the approach of building the control architecture in parallel loops for each mode and every flap (see Figure 3) is the assumption of a linear aero-servoelastic flutter system modelling (ASE). Out of this, the conclusion of the superposition principle for modal signals can be drawn, in the sense that model linearity and further persisting validity of the superimposable modal approach has been assumed to be valid throughout the whole control loop. Note here that both, the controller TF_j and the gain values G_j depend on the respective flutter mode „j" only, and thus are equal for all flaps „i".

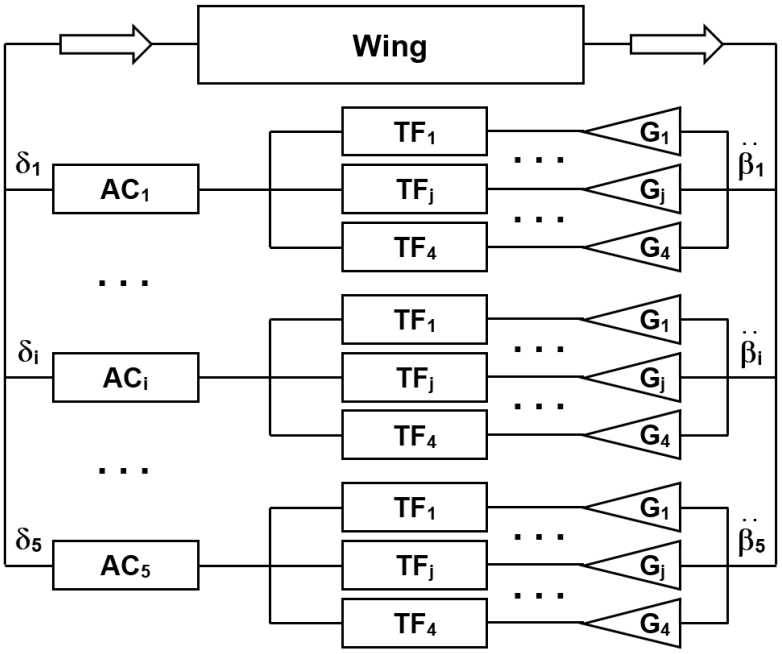

Figure 3: Control loop design, comprising gains (G), controllers (TF) and actuators (AC) – control variable flap deflection δ_i and sensor signal elastic wing pitch acceleration $\ddot{\beta}_i$.

5 CLOSED-LOOP FLUTTER ANALYSES

5.1 Design of the Actuators and Controller Type 1

As generic control elements equal for each of the five control surfaces, a flap actuator model was selected which already prior had been used for aircraft design purposes and whose dynamic transfer characteristics is defined by its transfer function (see Figure 4 and also Figure 15).

$$AC_i = \frac{1.}{s^3 + .000277\, s^2 + .013333\, s + 1.}$$

Figure 4: Actuator transfer function.

Because of the above mentioned expensive necessity of finding the parameters for the respective rational functions (plus the gain values), a transfer function with a simple structure had been chosen (see Figure 5) within the first approach. In order to find a control law for flutter mode 1, the values of the respective transfer function parameters had been determined in a heuristic approach by trial and error.

$$TF_1 = \frac{+48000.}{s - 454.49}$$

$$G_1 = 1.00$$

Figure 5: Controller type 1 and gain for flutter eigenmode 1.

5.2 Flutter Suppression with Controller Type 1 (Model Configuration I)

The impact of this controller type 1 together with wing configuration I in the closed-loop flutter calculation, defined to counteract flutter mode 1 (heave), is shown in this chapter. Beside the eigenmodes, the flutter diagrams as the most important results of the aeroelastic simulations are presented. The values of modal damping ratios and frequencies have been derived from the solution of the respective eigenvalue problems. The curves show the changing of the aeroelastic behaviour with respect to free stream velocity. An eventual sign change of the damping curves (when passing from the positive into the negative half of the diagram) especially indicates the loss of stability of the system. As a first example for active flutter suppression by addressing an individual flutter mode, the case of the heave flutter mode 1 of wing configuration I is presented. Here, the rotational acceleration signal around the chord length axis, α'' (around the global x-axis), at the wing tip had been taken as corresponding sensor value. Obviously sufficient, only the outermost control surface (flap no. 5) had been activated, while the inner flaps remained fixed to the wing structure. The respective controller transfer function (together with a gain of 1.) had been determined as shown in Figure 5. The results, presented as frequencies and damping ratios for the uncontrolled open-loop in Figure 6 and for the controlled closed-loop system in Figure 7 show how flutter case 1 (heave case; the blue curves) could be completely suppressed over the whole flight velocity range. As to mode 2, a broader approach has been chosen next.

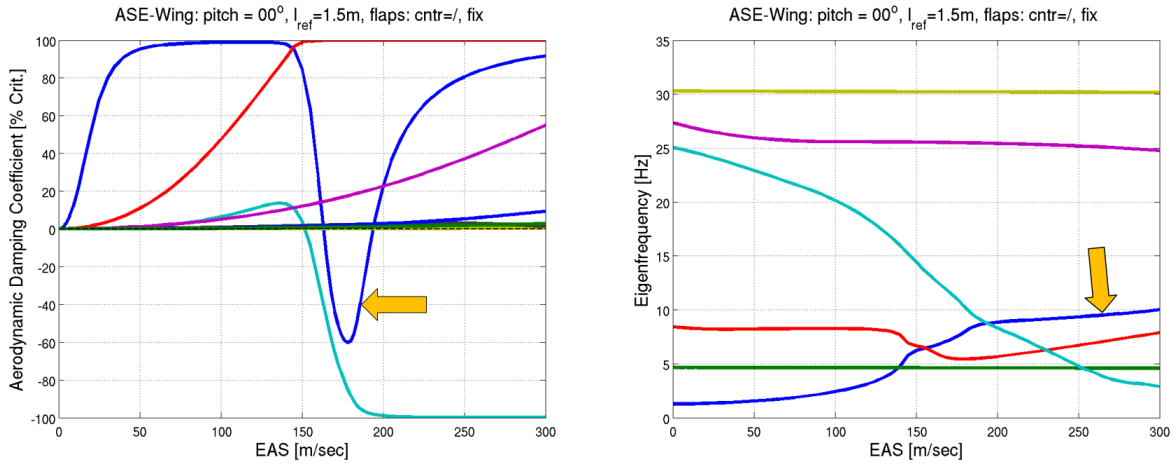

Figure 6: Flutter diagrams of wing configuration I – open loop: Arrows indicate flutter mode 1; damping ratios (left) and aeroelastic eigenfrequencies (right).

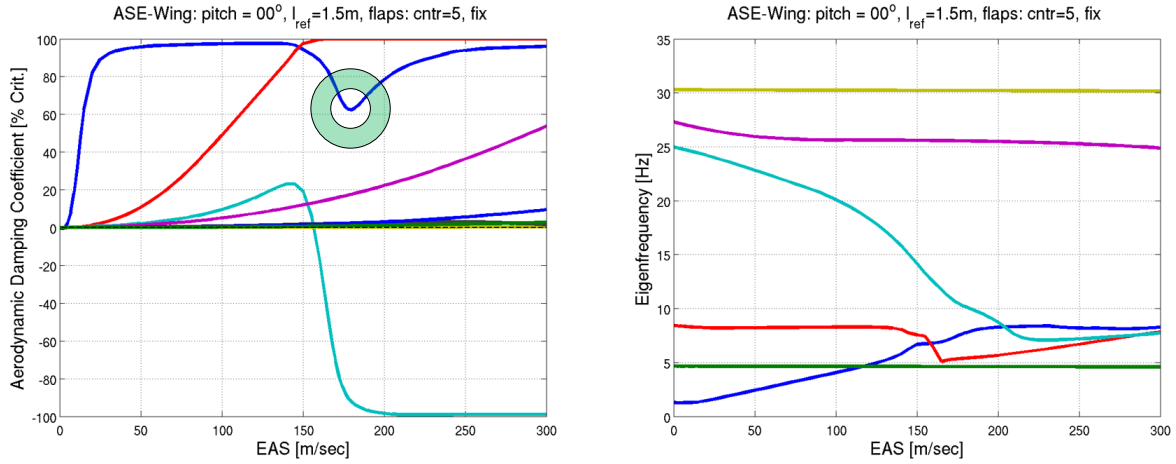

Figure 7: Flutter diagrams of wing configuration I – closed loop: Controlled mode 1; damping ratios (left) and aeroelastic eigenfrequencies (right).

5.3 Design of Controller Type 2

Although the controller type 1 (defined in Figure 5) perfectly fulfilled the purpose it had been designed for (suppressing the heave flutter mode), it exhibited a principle drawback. Comparing the damping and frequency curves (cyan) for the flutter mode 2 in Figure 6 and 7, an unintended small but obvious impact also on this torsional flutter mode can be perceived. To circumvent these unintended spillover effects which could hamper precisely addressing all of the individual flutter modes, a second type of controller, defined by a more complex transfer function had been determined and introduced (see Figure 8). The shape of this controller type does not only enable a more precise access to the particular flutter modes. By use of the respective flutter frequencies in the rational function, it also eases the determination of the transfer function parameters. With the controller structure in such a way "predefined", only the definition of a (sufficiently high) gain value remains as the final control law design task.

$$TF_j = \frac{s - \omega_{\text{j\_flut}}}{s^2 + 0.04\,\omega_{\text{j\_flut}}\,s + \omega_{\text{j\_flut}}{}^2}$$

Figure 8: Controller type 2, general form.

$$TF_1 = \frac{s - 43.637}{s^2 + 1.7455\,s + 1904.2} \qquad G_1 = 7.5624$$

$$TF_2 = \frac{s - 83.818}{s^2 + 3.3527\,s + 7025.4} \qquad G_2 = 31.020$$

$$TF_3 = \frac{s - 27.891}{s^2 + 1.1156\,s + 777.91} \qquad G_3 = 0.53781$$

$$TF_4 = \frac{s - 207.53}{s^2 + 8.3013\,s + 43070.} \qquad G_4 = 4.1921$$

Figure 9: Controller type 2 and gain for flutter eigenmodes 1 – 4.

5.4 Flutter Suppression with Controller Type 2 (Model Configuration III)

Together with the above defined sensor and actuator characteristics, the controllers for the four flutter modes presented in Figure 9 were incorporated into the global control loop structure from Figure 3. By activating or disengaging the control signals for the individual flutter modes, the respective unstable modes could be turned into stable, considerably damped aeroelastic eigenmodes. Thus, the initially defined task of suppressing all occurring flutter modes proved to be successfully fulfilled. The application of the complete control structure has been demonstrated in closed-loop flutter calculations for wing configuration III. The results in shape of flutter curves are presented sequentially in the following diagrams. Starting with the open-loop calculation (Figure 10), all four flutter cases are presented one after the other. The four flutter modes are suppressed in a row, starting with the heave mode (j=1, Figure 11), followed by the torsional mode (j=2, Figure 12), the swaying mode (j=3, Figure

13) and finally the flap dominated mode (j=4, Figure 14), resulting in the controlled, complete stable system.

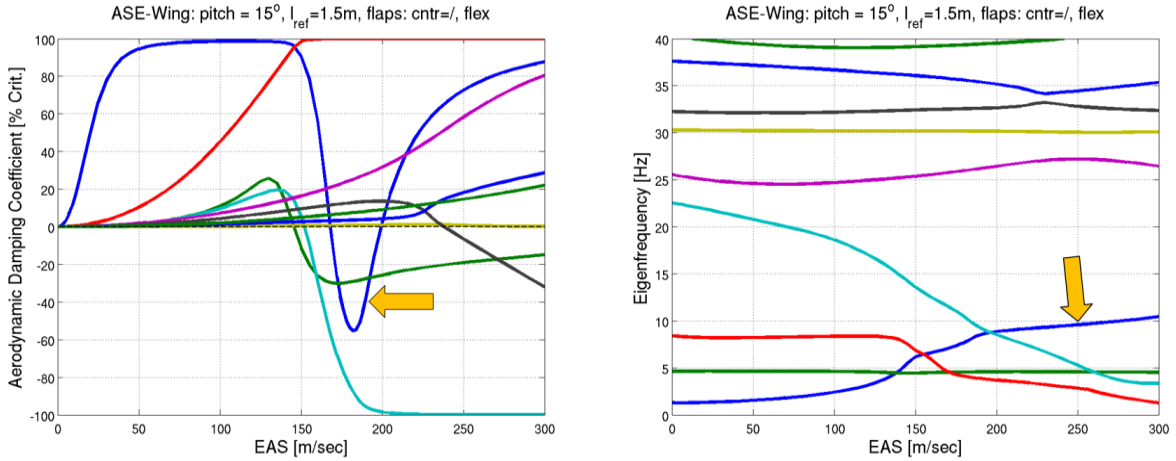

Figure 10: Flutter diagrams of wing configuration III – open loop: Arrows indicate flutter mode 1; damping ratios (left) and aeroelastic eigenfrequencies (right).

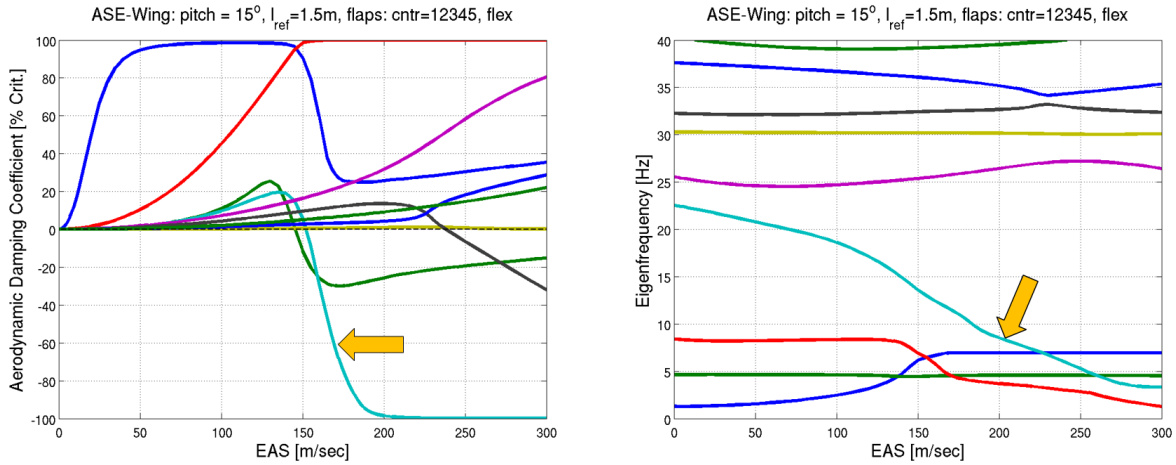

Figure 11: Flutter diagrams of wing configuration III – closed loop: Controlled mode 1; arrows indicate flutter mode 2; damping ratios (left) and aeroelastic eigenfrequencies (right).

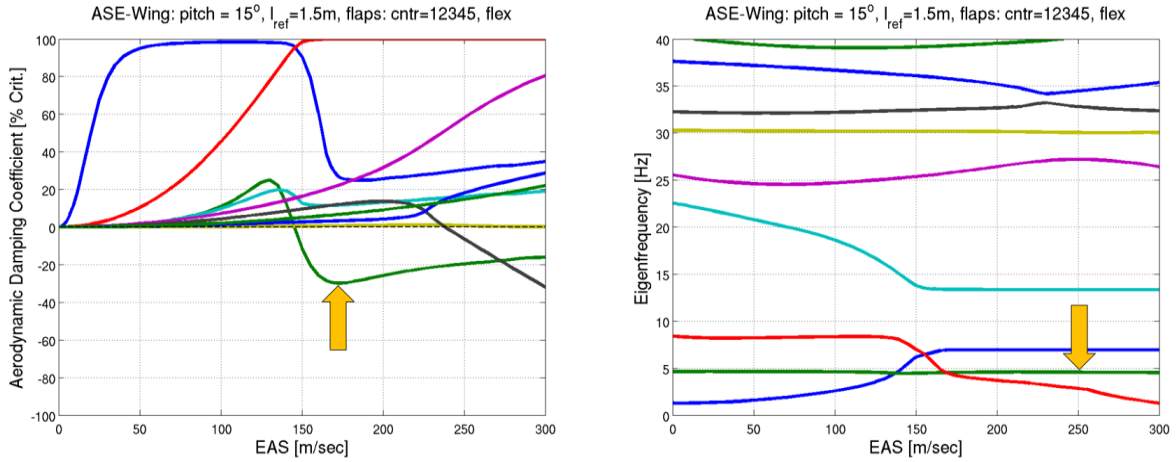

Figure 12: Flutter diagrams of wing configuration III – closed loop: Controlled modes 1 and 2; arrows indicate flutter mode 3; damping ratios (left) and aeroelastic eigenfrequencies (right).

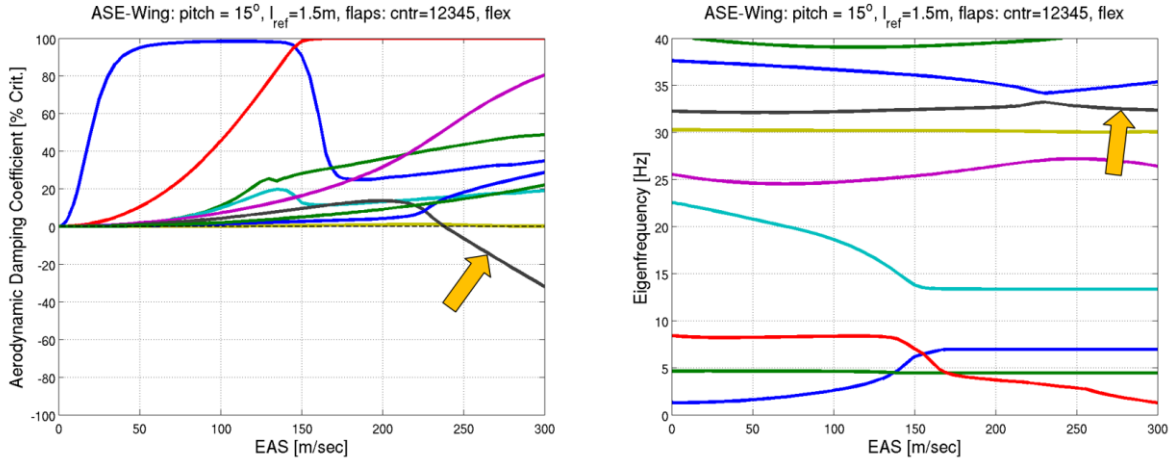

Figure 13: Flutter diagrams of wing configuration III – closed loop: Controlled modes 1, 2 and 3; arrows indicate flutter mode 4; damping ratios (left) and aeroelastic eigenfrequencies (right).

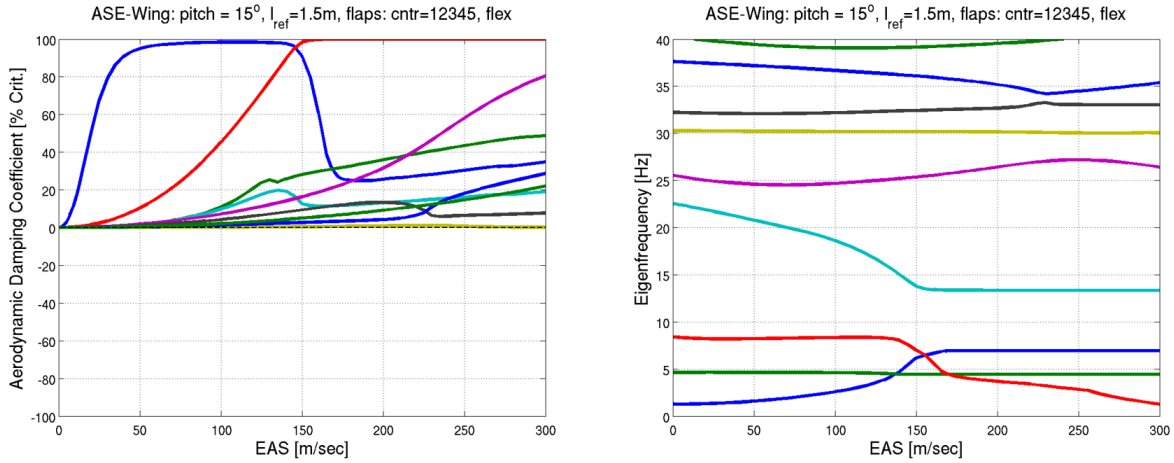

Figure 14: Flutter diagrams of wing configuration III – closed loop: Controlled modes 1, 2, 3 and 4; damping ratios (left) and aeroelastic eigenfrequencies (right).

6 CLOSED-LOOP CONTROL DYNAMICS

6.1 Controller Transfer Functions

Since in the linear modelling of the aero-servoelastic system no potentially nonlinear properties of the ASE control elements can execute a limiting impact on the effectiveness of the control loop, the question of the flap deflection amplitudes, necessary to achieve the intended flutter suppression goal, can be raised. Although eigenvalue solutions remain undetermined w.r.t. the mode amplitudes, the evaluation of the transfer functions for the complete control chain can render a hint for the amplification ratio. The complex actuator/controller functions in the loop (now with the sensor acceleration values transformed into deflection angles) have been evaluated in shape of magnitude and phase curves for configuration III, and are shown in Figures 15 and 16. The resulting amplification factor (magnitude) with a value of about 0.2 at the flutter frequency for flutter mode 2 (in Figure 15), means the local airfoil pitch deformation angle being roughly five times higher than the necessary counteracting flap deflection control angle (while this low control value, in a way, can also be considered as a justification for the linear model approach w.r.t. the deformation amplitudes).

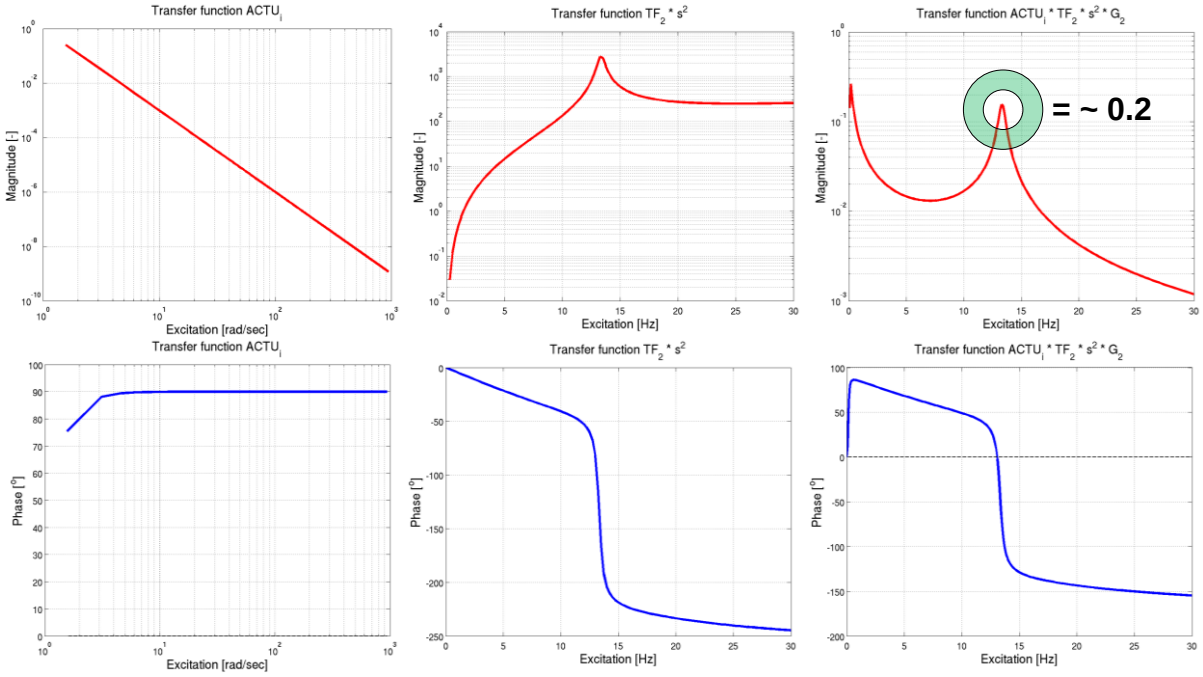

Figure 15: Transfer functions for the actuator (left), controller 2 (center) and total control loop (δ_i / β_i) of flutter mode 2 (right) of configuration III.

6.2 Total Control Loop Transfer Function

While in Figure 15 the composition of the total control loop transfer function for flutter mode 2 as product of the single actuator and controller transfer functions is shown, in Figure 16 the final, total transfer behaviour for the remaining flutter modes 1, 3 and 4 is presented. In case of rigid body modes, it could become relevant that for excitation 0 Hz the magnitudes of the transfer functions tend toward zero.

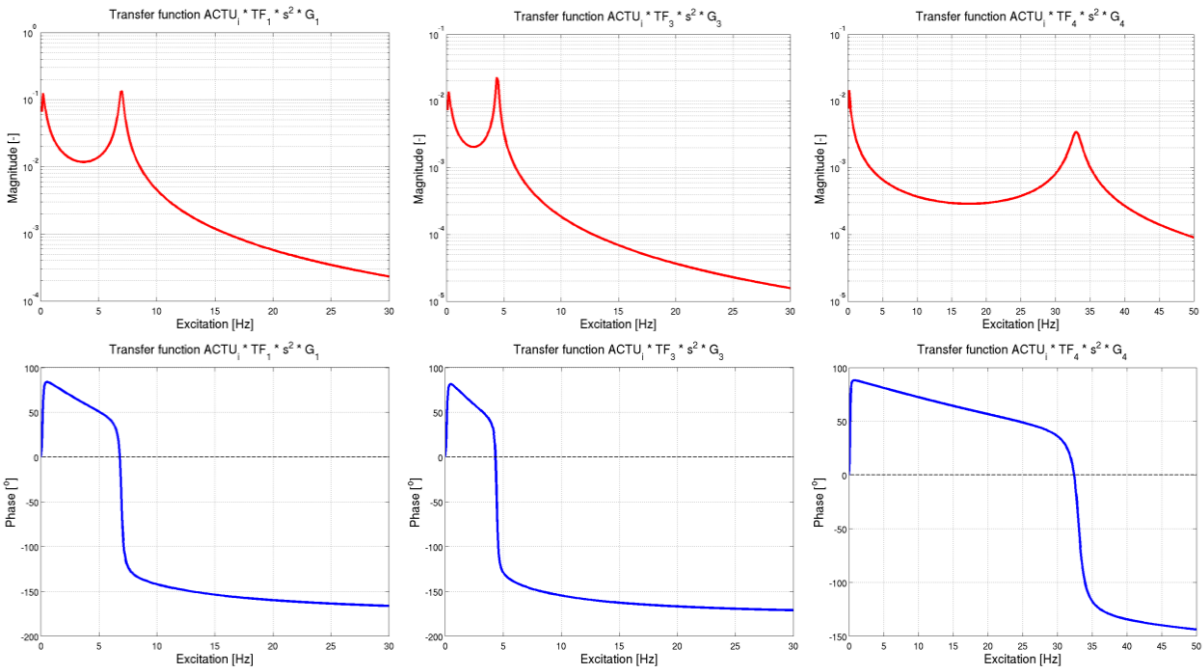

Figure 16: Total control loop transfer functions (δ_i / β_i) for flutter mode 1 (left), flutter mode 3 (center) and flutter mode 4 (right) of configuration III.

7 CLOSED-LOOP FLUTTER WITH REDUCED FLAP SUBSETS

7.1 Effectivity and Redundancy

Beside the control deflection amplitude of the flaps, the control surface area plays an important role in the controllability of flutter, and thus, the ability to suppress instabilities of aeroelastic modes varying along the wing span. In an additional parameter study, only reduced subsets of flaps were activated, while the remaining flaps had been taken out of the control loop. Starting at the wing root, the inner flaps sequentially had been switched of. Thus, the subsets of the remaining in-the-loop flaps had been assembled by the adjacent outer flaps. As results of the closed-loop flutter calculations with the controller type 2, the additional gain values in percentage of the nominal (five flap) control case, necessary to sustain the suppression of the respective mode, are shown in Table 5. High ΔG values indicate that the reduced number of flaps in the subsets had to be controlled with a larger amplitude, whereas the subsets with the unchanged gain 0% ΔG still remained stable, while being controlled by less flaps (i.e. with a smaller collective control surface area). It can be perceived that the ΔG result values differ quite strongly between the single modes.

Generally, it can be concluded that the control of flap subsets with high ΔG values is not as effective as the low or 0% ΔG value cases for the respective flutter mode (and probably could be improved in effectivity by allowing further flap combinations). On the other hand, the 0% ΔG subset cases proved most robust, capable of suppressing the flutter case even with the reduced number of flaps. As most pronounced example, concerning the heave mode (j=1), the activation of only the outermost flap evidently is sufficient, whereas, on the other hand, taking more (or all five) flaps into the control loop would result in an increase of "redundancy" against flutter instability, with the deflection angle amplitude remaining unchanged.

Table 5: Closed-loop flutter suppression with controller type 2: Necessary additional gain in case of controlled flap number reduction (w.r.t. the nominal all in-the-loop case).

ΔG_j	Flutter mode j = 1	Flutter mode j = 2	Flutter mode j = 3	Flutter mode j = 4	Controlled flaps
Flap i = 1	+0 %	+0 %	+0 %	+0 %	All flaps (nom.)
Flap i = 2	+0 %	+0 %	+0 %	+0 %	Flap 2, 3, 4, 5
Flap i = 3	+0 %	+0 %	+0 %	+195 %	Flap 3, 4, 5
Flap i = 4	+0 %	+30 %	+15 %	+185 %	Flap 4, 5
Flap i = 5	+0 %	+265 %	+100 %	+700 %	Flap 5

Finally (and not further investigated), another aspect for enlarging the effectivity of control loop could lie in the adaptation of the controller transfer functions not only to the targeted mode, but also to the individual flap ($TF_j \rightarrow TF_{ij}$, see Figure 3). By using a "local" control loop between the individual sensor signals and the respective flap deflection as done here, at least a local dependency between sensor and actuator is guaranteed (collocated feedback), which at the end proved to be sufficient for the ASE wing demonstrator investigated in this study.

8 CONCLUSIONS

As investigation results of this project, the chosen AFS approach has been demonstrated to be suitable to cope simultaneously with any kind or number of aeroelastic dynamic instabilities of slender and flexible wing structures. Effective flap controllers for the suppression of flutter cases could be designed through simulations. By individually counteracting the respective eigenmodes, the capability of removing the connected flutter instabilities to higher flight

speed regions or wipe out them at all has been achieved. The structure of the complete control chain has been presented in the paper together with the final results. Limitations in predicting the aero-servoelastic stability behaviour are based on the linearity of the approach and the superposition principle of the applied structural modelling, as well as the physical regime of the unsteady aerodynamics (subsonic regime) which had been covered in this study. Geometric or physical non-linearities (e.g. actuator saturation [3]) have been neglected in the systematic approach to design an active flutter suppression control loop.
By actively suppressing any kind and number of flutter mode shapes over any desired flight velocity range, the main goal of active flutter suppression for the chosen wing configurations has been reached in this study. Prerequisites proved mainly to be appropriate controller transfer functions which in turn, keep the closed-loop control insensitive toward small gain variations and limit the necessary flap deflection angles to moderate values. Flutter suppression with subsets of less flaps involved was shown to be possible, but with potentially rising gain values. As an outlook, proceeding work could comprise further optimization of the individual flutter mode control (e.g. selection of controlled flap subsets) and extension from the mode dependency for gain G_j and transfer functions TF_j toward also an individual flap dependency (to G_{ij} and TF_{ij}). Further investigation could deal with the influence of local modes (engine nacelle), flutter frequency proximity, aerodynamic flap effectivity and transonic aerodynamics.

9 ACKNOWLEDGMENT

The investigation work for this study has been conducted within the DLR project oLAF (Optimal Lastadaptives Flugzeug / Optimally Load-adaptive Aircraft), run-time 2020 – 2023.

10 REFERENCES

[1] ZAERO User's Manual, Version 9.2, Zona 02 – 12.4, Zona Technology Inc., Jan. 2016.

[2] ZAERO Theoretical Manual, Version 9.2, Zona 02 – 12.4, Zona Techn. Inc., Nov. 2016.

[3] Micheli, B. 2022, "Active Flutter Suppression of a Two-dimensional Airfoil with Actuator Saturation", IFASD 2022, Madrid, Spain.

[4] Waitman, S. and Marcos, A. 2020. H∞ Control Design for Active Flutter Suppression of Flexible-Wing Unmanned Aerial Vehicle Demonstrator. Journal of Guidance, Control, and Dynamics 43, 4, 656–672.

[5] Theis, J., Pfifer, H., and Seiler, P. 2020. Robust Modal Damping Control for Active Flutter Suppression. Journal of Guidance, Control, and Dynamics 43, 6, 1056–1068.

[6] Schmidt, D.K. 2016. Stability Augmentation and Active Flutter Suppression of a Flexible Flying-Wing Drone. Journal of Guidance, Control, and Dynamics 39, 3, 409–422.

[7] Haley, P. and Soloway, D. 2001. Generalized Predictive Control for Active Flutter Suppression. Journal of Guidance, Control, and Dynamics 24, 1, 154–159.

[8] Bernelli-Zazzera, F., Mantegazza, P., Mazzoni, G., and Rendina, M. 2000. Active Flutter Suppression Using Recurrent Neural Networks. Journal of Guidance, Control, and Dynamics 23, 6, 1030–1036.

[9] Tewari, A. 1998. Robust optimal controllers for active flutter suppression. American Institute of Aeronautics and Astronautics, AIAA 1998.

[10] Ghiringhelli, G.L., Lanz, M., and Mantegazza, P. 1990. Active flutter suppression for a wing model. Journal of Aircraft 27, 4, 334–341.

[11] Karpel, M., “Sensitivity Derivatives of Flutter Characteristics and Stability Margins for Aeroservoelastic Design,” Journal of Aircraft, Vol. 27, No. 4, 1990, pp. 368-375.

[12] Liebst, B.S., Garrard, W.L., and Adams, W.M. 1986. Design of an active flutter suppression system. Journal of Guidance, Control, and Dynamics 9, 1, 64–71.

[13] Karpel, M., “Design for Active Flutter Suppression and Gust Alleviation Using State-Space Aeroelastic Modeling,” Journal of Aircraft, Vol. 19, No. 3, 1982, pp. 221-227.

[14] Albano, E. and Rodden, W.P. 1969. A doublet-lattice method for calculating lift distribution on oscillating surfaces in subsonic flow. *Journal of Aircraft*, 7(2), 279-281.

COPYRIGHT STATEMENT